onsemi™

Automotive 3 μm HDR Image Sensor With LFM and Distance Functionality

Automotive 3 μm HDR Image Sensor With LFM and Distance Functionality

Sergey Velichko⬤, Dave Jasinski, Michael Guidash, Daniel Tekleab, Manuel Innocent, Andrew Perkins⬤, Shaheen Amanullah, Maheedhar Suryadevara, Chris Silsby, and Jeff Beck

Abstract—We described a 3 μm super-exposure pixel 1.3-MP CMOS image sensor for automotive application that provided for up to 140 dB high dynamic range (HDR) coverage with multiexposure operation, as well as effective HDR with LED flicker mitigation (LFM) operation. At junction temperatures in excess of +100 °C, total signal-to-noise transitions were kept at or above 30 dB due to further development of the pixel pulsed gate operation and process optimization. Pulsed LFM operation provided for capturing flickering lights of any brightness. Two-photodiode pixel architecture in combination with single microlens covering the pixel also enabled distance extraction along with a color image using in-pixel phase detect.

Index Terms—CMOS, distance, high dynamic range (HDR), image sensor, LED flicker mitigation (LFM).

Fig. 1. SE two PDs' DCG pixel schematic.

I. INTRODUCTION

LATEST automotive image sensors are addressing challenging street scenarios with flickering LEDs and high dynamic range (HDR). Classical multiexposure image sensor architecture [1] was developed and HDR reached in excess of 140 dB [2] with junction temperatures up to +125 °C. Image sensor architectures addressing both HDR and LED flicker mitigation (LFM) were developed using pulsed pixel operation [3] and split-diode pixel architectures [4]–[6]. These solutions achieved good LFM capabilities but resulted in reduced image quality, especially at high automotive temperatures. Earlier concept of lateral overflow integrating capacitor (LOFIC) architecture [7], [8] was significantly changed and modified for automotive use [9], [10] providing high-performance HDR with LFM even at high automotive temperatures. These new automotive image sensors are powering the latest advancements in autonomous and assisted driving as well as better viewing applications such as surround and rear view, e-mirror, digital video recording, and augmented reality displaying. Some applications also require fused image and distance data using the same camera solutions.

II. PIXEL DESIGN

We designed and tested a 3 μm pixel 1.3-MP CMOS imager that provides cinematographic HDR image quality even for high temperatures with all signal-to-noise ratio (SNR) transitions at or above 30 dB. Two photodiodes (PDs) dual conversion gain (DCG) eight-gate pixel schematic is presented in Fig. 1.

The sensor implemented a set of operations effectively as follows:

1) four-exposure 140 dB HDR image captures [2];
2) pulsed LFM (pLFM) [3] using shutter gates SGA and SGB, transfer gates TXA and TXB, and an in-pixel memory node comprised of floating diffusion (FD), DCG gate, and capacitor C;
3) super-exposure (SE) LOFIC HDR LFM [9], [10] using TXA and TXB in conjunction with the memory node;
4) distance extraction along with a color image using in-pixel phase detect by utilizing signal levels from two PDs PDA and PDB covered by a single microlens [11].

In the pixel, reset gate (RST) and SGA/SGB gates are used for resetting PDs PDA and PDB, as well as the memory node FD and C. Source follower (SF) and row select (RS) gates are used to connect the pixel to the column circuitry for readout sequences.

TCAD potential profile simulation of the pixel's two PDs and gates is presented in Fig. 2 confirming complete charge transfer and PD-to-PD extremely low crosstalk characteristics. In the simulation one, PD is being readout, while another
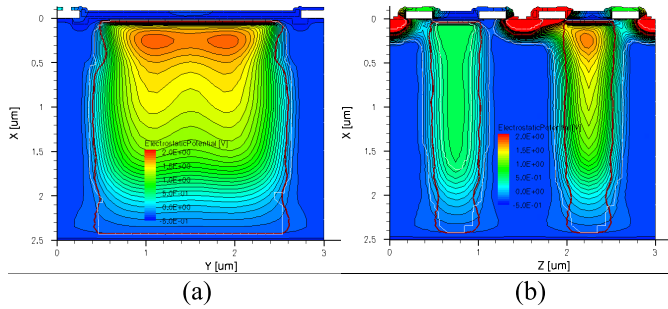
Fig. 2. TCAD potential profile simulation for pixel's two PDs and gates. (a) Side view and (b) cross-sectional view.
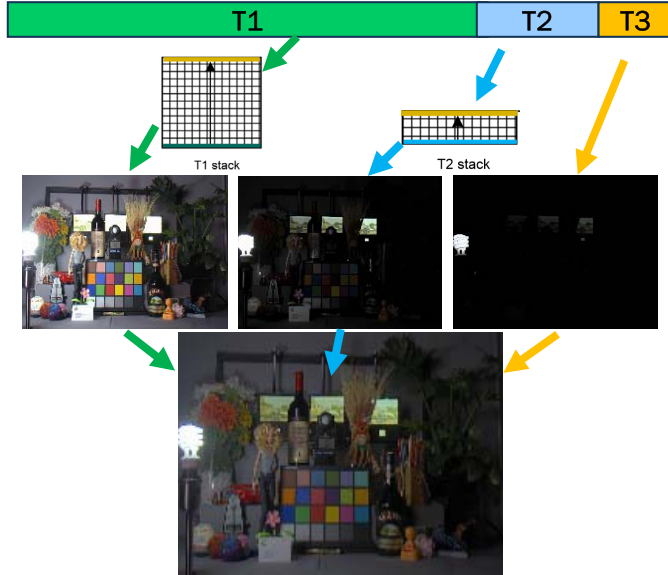

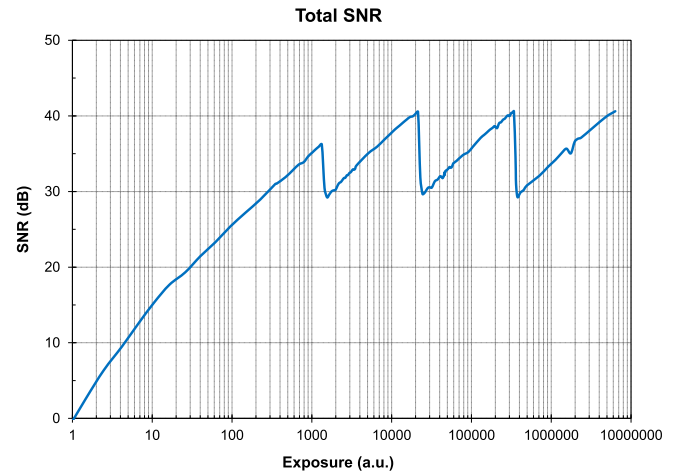Fig. 3. Multiexposure HDR schema with delay buffers.

Fig. 4. Four-exposure room temperature 140 dB dynamic range total SNR with HCG T1, LCG T2, LCG T3, and LCG T4 exposure readout.
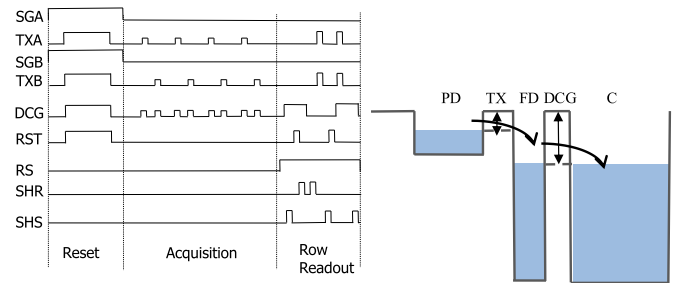

Fig. 5. SE LFM pixel timing and potential diagrams.

PD is still holding acquired photon-generated charge. Fig. 2(a) shows the cross section of the PD being readout and some of the RST, SF, DCG, and RS gates in the periphery. Fig. 2(b) shows the TXA/TXB gates in the center and SGA/SGB gates on the periphery, left PD is holding charge, and right PD is being readout.

III. MULTIEXPOSURE HDR

Multiexposure implementation followed classical HDR schema [1] with delay buffers (Fig. 3). T1 stack and T2 stack memory buffers are used to hold digital values of the pixel signal acquired during first longer T1 and second shorter T2 exposures, respectively. These buffers are located in-sensor and used during HDR per pixel signal recombination. At the end of the third shortest exposure T3, all three pixel values were combined into an HDR multibit value, usually 20 bit for three exposures or 24 bit for four exposures (with additional T3 stack memory). Thus, three exposures allowed up to 120 dB and four exposures allowed up to 140 dB-HDR in frame image captures.

Characterization of four-exposure HDR mode at room temperature showed a 140 dB dynamic range and all total SNR transitions at or above 30 dB with first T1 exposure readout using high conversion gain (HCG) (Fig. 4).

Combination of HCG T1 with low readout noise and low conversion gain (LCG) T2, T3, and T4 readout with extended dynamic range provided for both excellent low and mid-to-high light performance while covering seven decades of light and exposure HDR.

IV. HDR WITH LFM

While classical multiexposure HDR provides for excellent performance with static sceneries, it does suffer from motion and LED flicker artifacts. We continued our previous work on the pixel SE LOFIC operation [9], [10] with further improvement for high ambient temperatures. New timing and potential diagrams of the pixel LOFIC HDR operation are shown in Fig. 5. Mid-level pulsed operation of the TX and DCG gates during charge acquisition and further process optimization reduced the memory node dark noise contribution in comparison to earlier work [9], [10] and thus improved SNR transitions for high temperatures. By keeping TX and DCG gate interface surfaces in the inverted state most of the acquisition time, the PD's and memory node dark current and dark signal nonuniformity (DSNU) were improved.

Mid-level pulsed parallel operation of the TX and DCG gates during charge acquisition provided also additional antiblooming protection.

During the readout phase, acquired charge in the memory node was readout in double-sampling mode [first sample-and-hold signal (SHS) and first sample-and-hold reset (SHR)] followed by readout of charge in both PDs using HCG (second

This article has been accepted for inclusion in a future issue of this journal. Content is final as presented, with the exception of pagination.

VELICHKO *et al.*: AUTOMOTIVE 3 μm HDR IMAGE SENSOR WITH LFM AND DISTANCE FUNCTIONALITY
3

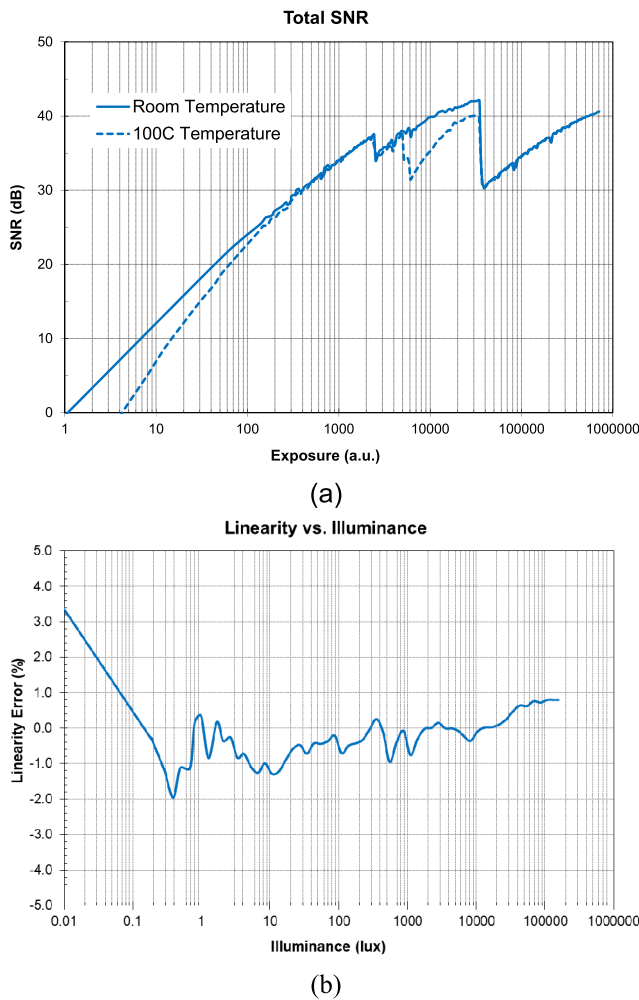(a)

Total SNR

(b)

Linearity vs. Illuminance

Fig. 6.   (a) SE 120 dB dynamic range total SNR versus temperature for 16-ms integration time and (b) pixel HDR LFM signal linearity versus lux illuminance.

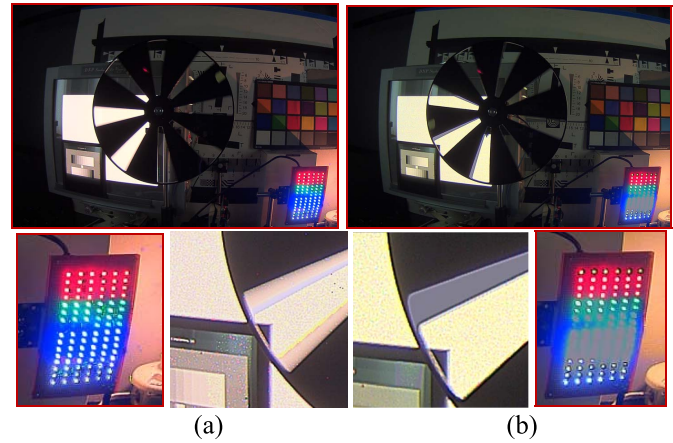(a)   (b)

Fig. 7.   Flickering LED and motion artifacts image comparison: (a) SE HDR LFM versus (b) three-exposure HDR.

Fig. 8.   pLFM pixel timing and potential diagrams.

SHR and second SHS) and LCG (first SHR and third SHS) correlated double-sampling techniques.

The total SNR comparison of room versus +100 °C junction temperature in Fig. 6(a) reflected sensor's 120 dB HDR LFM performance.

This mode of operation also provided for excellent image quality with all total SNR transitions at or above 30 dB for +100 °C and 16-ms integration time [Fig. 6(a)] and even for +125 °C and shorter 8-ms integration time. High performance at elevated temperatures achieved via further process and pixel operation optimization controlling the memory node dark current and DSNU that changed significantly between room and +125 °C temperatures [9], [10]. The first SNR transition happened between readout of PDs signal in the HCG mode and readout in the LCG mode due to higher LCG readout noise, and the second SNR transition had added pixel memory dark current and DSNU that were temperature and integration time dependent. While the readout noise of double-sampling readout caused some reduction of SNR in second transition at room temperature, but it was not a significant factor at high temperature where memory node dark current and DSNU

were dominant. The third SNR transition was between first and very short second exposure. The ratio between first and second exposures controlled how deep the SNR reduction could be. Thus, the third SNR transition was not temperature-dependent.

Linearity measurements from 0.01 lx to almost 200 K lux showed excellent color reproducibility by staying within +1% to −1.5% of signal, from less than 0.5 lx to max level in Fig. 6(b). Pixel's SE HDR LFM operation captured bright flickering LEDs and eliminated motion artifacts in comparison to classical multiexposure HDR [Fig. 7(a) versus (b)].

The pLFM method that we developed earlier [3] and implemented in the sensor allowed capturing flickering light sources of any brightness up to millions of lux. The pLFM operation timing diagram is shown in Fig. 8.

In Fig. 8, TXA/TXB and SGA/SGB gates are fully pulsed during charge acquisition in a push–pull manner [3]. Their duty cycles regulate electronic PD responsivity in a wide range as well as charge summing accumulation in the memory node. DCG gate may be pulsed as shown to allow capacitor *C* to connect to the overflow path via the FD and thus extend dynamic range of the captured pLFM image. DCG gate may also be asserted for the entire length of the charge acquisition. Different pulse timing of TXA/SGA and TXB/SGB pairs created much higher sampling frequency and thus better capturing of very low duty cycle LED pulses that could be captured at least by one PDA or PDB.

Fig. 9.   Flickering LED turn lights, headlights, and brake lights image captures three-exposure HDR (top) versus pLFM HDR (bottom).
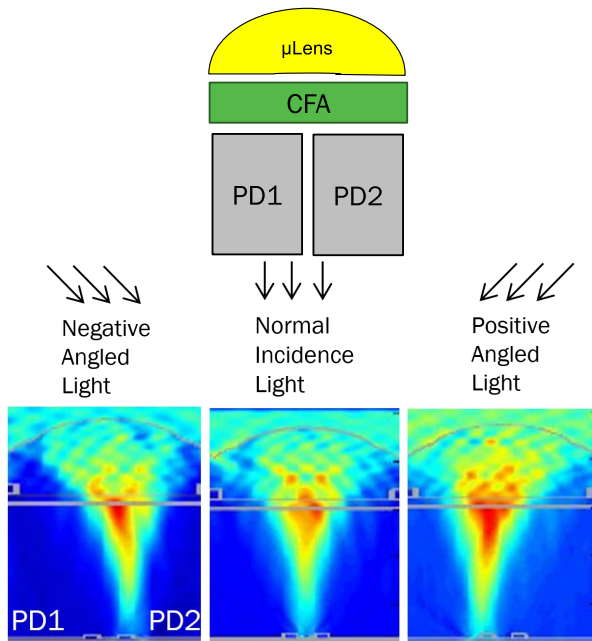

Fig. 11. Pixel array geometrical optics construction for phase detect.

Fig. 10.   Phase detect pixel with two PDs and its FDTD optical simulation versus light angles.
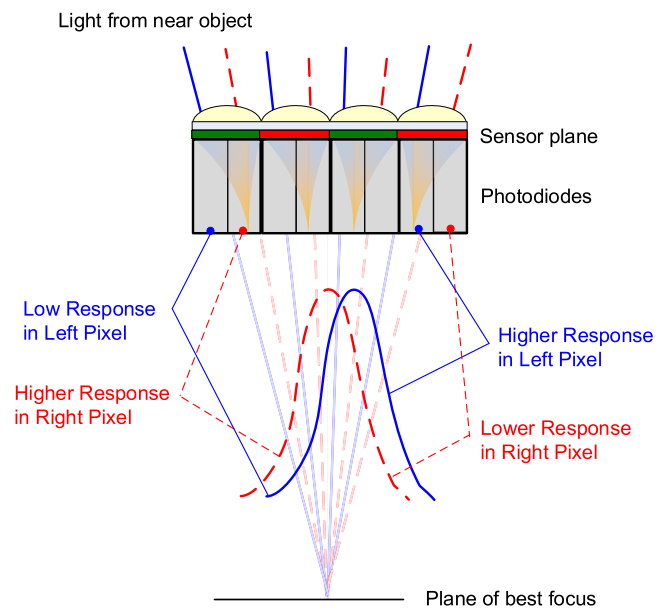
Fig. 12. Different response in the phase detect pixels PDs.

During the readout phase, acquired charge in the memory node was readout in double-sampling mode (first SHS and first SHR) followed by HCG correlated double-sampling readout (second RST and second SHS) of the remaining charge in both PDs.

Image comparison of capturing flickering LED turn lights, headlights, and brake lights using three-exposure HDR and pLFM are shown correspondingly in the top and bottom images of Fig. 9. These images confirmed effective capturing of automotive LED light sources in true color.

V. DISTANCE AND IMAGE SIMULTANEOUS ACQUISITION

Two-PD pixels in the sensor covered by a single microlens additionally enabled distance extraction along with a color image using in-pixel phase detect [11]. This was first application of two-PD in-pixel phase detect to HDR pixel architecture. Fig. 10 shows a finite-difference time-domain (FDTD) optical simulation of the pixel with two PDs in relation to angles of green light between $+30°$ and $-30°$.
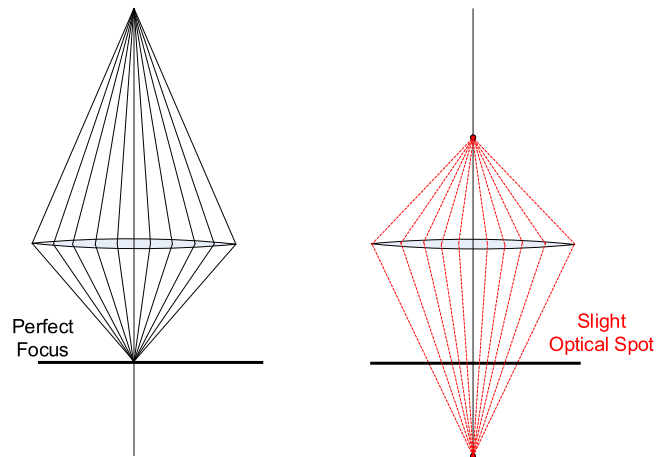
Objects at different distances from the imaging lens generate differences in the signal acquired by each of two PDs within the pixel.

Fig. 11 shows the principle of the phase mechanism using a geometrical optics construction. An object in perfect focus would form a perfect image point on the sensor plane producing zero phase. When an object is out of focus, its image point is beyond the sensor plane resulting in a cone of rays forming the circle of confusion at the sensor plane. Depending on the degree of defocus, the circle of confusion may span several pixels of the sensor array.

At each pixel PD location, the angle of the incoming ray is sensed by the phase-detect auto-focus (PDAF) sensor producing a phase response (Fig. 12). The following derivation considers the image of a point source, but in practice, phase measurements are derived from the analysis of edges in the scene.

Fig. 13 shows the basic principles of phase generation that can be derived from geometrical optics. For the derivation
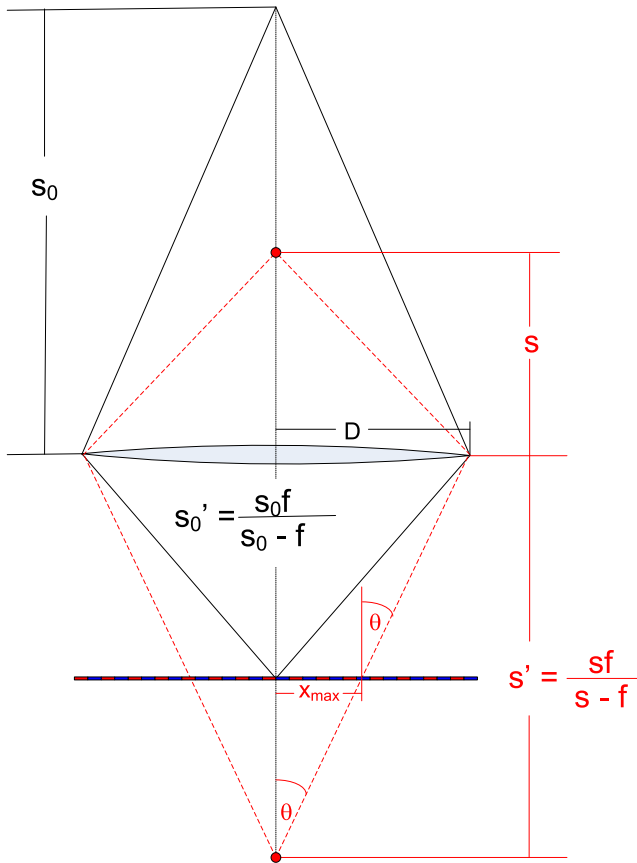
This article has been accepted for inclusion in a future issue of this journal. Content is final as presented, with the exception of pagination.

VELICHKO *et al.*: AUTOMOTIVE 3 μm HDR IMAGE SENSOR WITH LFM AND DISTANCE FUNCTIONALITY

5

Fig. 13. Geometrical derivation of near defocus response.

Fig. 14. Pixel depth range versus lens *f*-number and focal length.

Fig. 15. Captured color image and corresponding signal phase/distance (close objects are reddish and distant objects are bluish).

of the phase displacement, we consider a lens focused on an object at a distance S_0. This places the image plane at a distance of S_0'. A point source closer to the lens will be out of focus creating a blur circle at the focal plane of the imager. For simplicity, we assume that all pixels within the blur circle are uniformly illuminated and those outside receive no photons, although in reality, diffraction effects will cause the blur circle to have some Gaussian-like intensity distribution.

D is one half of the clear aperture of the lens. By definition of the *f*-number of a lens, N is equal to the focal length over the clear aperture diameter. By similar triangles, the maximum extent $X_{\max}$ of the blur circle may be expressed as

$$X_{\max} = \frac{f(s' - s_0')}{2Ns'}. \tag{1}$$

For any point on the sensor array across the extent of the blur circle, we can calculate the angle of the light ray from an out of focus point as follows:

$$\theta = \tan^{-1}\left(\frac{x}{s' - s_0'}\right). \tag{2}$$

Based on the above derivation in (1) and (2), we conclude that both the extent of the optical spot and the angles of the incoming rays are dictated by the diameter of the entrance pupil, which is directly related to the lens *f*-number and the lens focal length, and thus, the depth capabilities are directly analogous to the depth of field characteristics of the lens. Wide-angle lenses with large depth of field in which all objects are effectively in focus provide very little phase information
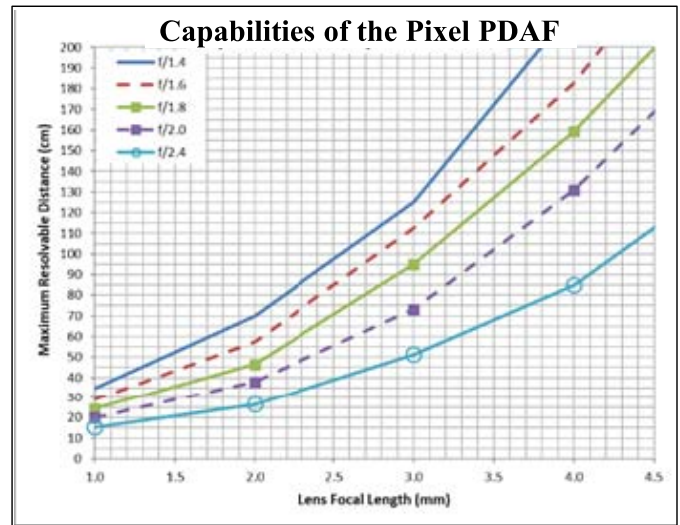
and thus have limited depth range. Telephoto lenses with longer focal lengths and lower *f*-numbers will have shallower depth of field allowing adequate phase information to be measured from more distant objects. However, there is a practical limit where near objects become too blurred to be adequately measured. Fig. 14 shows the pixel distance performance characteristics for different lens *f*-numbers and focal length.

Two-PD implementation of same-color pixels under a single microlens allowed effective distance extraction using edges of different objects in sceneries. Both color HDR image and distance information of up to a few meters could be acquired with reasonable accuracy as shown in Fig. 15, where right image distance data red color showed objects closer and blue color showed objects farther from the camera.

This additional feature is valuable for some automotive in-cabin and close proximity applications that require fusion of distance and image data.

VI. PERFORMANCE COMPARISONS

Some of the latest HDR LFM backside-illuminated (BSI) pixel performance metrics are summarized in Table I. In the table, different architecture pixel types were captured as well as some of their major parameters: pixel linear full-well (LFW) capacity, maximum dynamic range, LFM HDR, maximum SNR in transitions versus temperature, and available modes of operation.

This article has been accepted for inclusion in a future issue of this journal. Content is final as presented, with the exception of pagination.

6   IEEE TRANSACTIONS ON ELECTRON DEVICES

TABLE I

MAJOR PARAMETER COMPARISON OF LATEST HDR LFM PIXELS

	THIS WORK	[10]	[4]	[5]	[6]
Pixel Size	3.0 µm	3.0 µm	3.0 µm	3.0 µm	2.8 µm
Architecture	SE dual-PD LOFIC	SE LOFIC	Split-diode	Split-diode	Split-diode
Technology	BSI	BSI	BSI	BSI	BSI
Pixel LFW	175 Ke-	140 Ke-	78 Ke-	165 Ke-	22 Ke-
Dynamic Range	140 dB	120 dB	~110 dB	130 dB	120 dB
HDR LFM	120 dB	120 dB	~110 dB	120 dB	120 dB
Max SNR in Transitions	30 dB @ 100°C 30 dB @ 125°C & 8 ms	25 dB @ 100°C ~20 dB @ 125°C	<18 dB @ 100°C <15 dB @ 125°C	~25 dB @ 100°C <20 dB @ 125°C	<23 dB @ 100°C <18 dB @ 125°C
Modes of Operation	HDR LFM 4-exp HDR pLFM Distance	HDR LFM	HDR LFM	HDR LFM	HDR LFM

In Table I, some of the parameters were extracted from plots or deduced using other parameters. Symbols "~" and "<" were used in these cases.

VII. CONCLUSION

We discussed the performance and features of the 1.3-MP automotive HDR image sensor based on enhanced 3 μm pixel with two PDs and eight gates. The pixel architecture allowed the implementation of multiple operation modes, including multiexposure HDR, SE LOFIC HDR LFM, and pLFM. These modes covered entire range of typical automotive sceneries and allowed effective mitigation of flickering LEDs and lights. Dynamic range achieved up to 140 dB with all total SNR transitions at or above 30 dB even for greater than +100 °C junction temperatures. In combination with HCG, low light signal readout that provided for a cinematographic image quality with sharp high color fidelity captures due to linearity between +1% and −1.5% of signal from very low to very bright light levels.

Additional mode of operation in conjunction with two PDs covered by a single microlens enabled up to few meter distance extraction along with a color image using in-pixel phase detect mechanisms.

Our future work is focused on smaller and better performing HDR LFM pixels that are based on the same architectural principals.

REFERENCES

[1] J. Solhusvik *et al.*, "A 1280×960 3.75 μm pixel CMOS imager with triple exposure HDR," in *Proc. Int. Image Sensor Workshop*, Jun. 2009, pp. 344–347.

[2] S. Velichko *et al.*, "140 dB dynamic range sub-electron noise floor image sensor," in *Proc. Int. Image Sensor Workshop*, Jun. 2017, pp. 294–297.

[3] C. Silsby, S. Velichko, S. Johnson, Y. P. Lim, R. Mentzer, and J. Beck, "A 1.2 MP 1/3' CMOS image sensor with light flicker mitigation," in *Proc. Int. Image Sensor Workshop*, Jun. 2015, pp. 405–408.

[4] S. Iida *et al.*, "A 0.68e-rms random-noise 121 dB dynamic-range sub-pixel architecture CMOS image sensor with LED flicker mitigation," in *IEDM Tech. Dig.*, Dec. 2018, pp. 2–10.

[5] Y. Sakano *et al.*, "A 132 dB single-exposure-dynamic-range CMOS image sensor with high temperature tolerance," in *IEEE Int. Solid-State Circuits Conf. (ISSCC) Dig. Tech. Papers*, Feb. 2020, pp. 105–107.

[6] J. Solhusvik *et al.*, "A 1280×960 2.8 μm HDR CIS with DCG and split-pixel combined," in *Proc. Int. Image Sensor Workshop (IISW)*, 2019, pp. 254–257.

[7] S. Sugawa *et al.*, "A 100 dB dynamic range CMOS image sensor using a lateral overflow integration capacitor," in *IEEE Int. Solid-State Circuits Conf. (ISSCC) Dig. Tech. Papers*, Feb. 2005, pp. 352–353.

[8] Y. Sakano *et al.*, "224-ke saturation signal global shutter CMOS image sensor with in-pixel pinned storage and lateral overflow integration capacitor," in *Proc. Symp. VLSI Circuits*, Jun. 2017, pp. C250–C251.

[9] M. Oh *et al.*, "3.0 μm backside illuminated, lateral overflow, high dynamic range, LED flicker mitigation image sensor," in *Proc. Int. Image Sensor Workshop*, Jun. 2019, pp. 262–265.

[10] M. Oh *et al.*, "Automotive 3.0 μm pixel high dynamic range sensor with LED flicker mitigation," *Sensors*, vol. 20, no. 5, p. 1390, 2020.

[11] S. Choi *et al.*, "An all pixel PDAF CMOS image sensor with 0.64 μmx1.28 μm photodiode separated by self-aligned in-pixel deep trench isolation for high AF performance," in *Proc. Symp. VLSI Technol.*, Jun. 2017, pp. T104–T105.

PUBLICATION ORDERING INFORMATION

◊